Vacuum 230 (2024) 113642

Contents lists available at ScienceDirect

Vacuum

journal homepage: www.elsevier.com/locate/vacuum

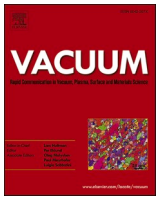

Investigation of spitting effect in the boron target preparation using vapour deposition technique

R. Mondal Saha [a], K. Banerjee [a,b,*], A. Banerjee [b,c], N. Gayathri [a,b], G. Pramanik [d], Shabi Thankaraj Salammal [e,f], Varsha Agrawal [e,f], Biswarup Satpati [b,c], Souvik Jana [b,c], Satyajit Hazra [b,c]

[a] Variable Energy Cyclotron Centre, 1/AF Bidhannagar, Kolkata, 700064, India
[b] Homi Bhabha National Institute, Training School Complex, Anushakti Nagar, Mumbai, 400094, India
[c] Saha Institute of Nuclear Physics, 1/AF Bidhannagar, Kolkata, 700064, India
[d] UGC-DAE Consortium for Scientific Research, Kolkata Centre, Sector III, LB-8, Bidhannagar, Kolkata, 700106, India
[e] CSIR-Advance Materials and Process Research Institute, Bhopal, 462026, India
[f] Academy of Scintific and Innovative Research, Gaziabad, 201002, India

ARTICLE INFO

Handling Editor: Prof. L.G. Hultman

Keywords:
Boron target fabrication
Vapour deposition
Spitting effect
XRD
FTIR
TEM
XPS

ABSTRACT

Self-supported and carbon/aluminum-backed isotopically enriched thin boron targets were prepared by the vapour deposition technique using electron beam. To mitigate spitting effects observed during this process, boron powder was evaporated in both paste and pellet forms. Effective reduction of spitting was achieved by initially heating boron at low currents followed by its step-wise increase. Analysis of boron samples at various stages of evaporation was done by X-ray Diffraction (XRD) and Fourier-transform Infrared spectroscopy (FTIR). Direct exposure to high-energy electron beams contributed to a decrease in boron oxide and hydride compounds, thereby aiding in minimizing spitting. However, upon exposure to air, the evaporated film underwent surface oxidation, confirmed by Transmission Electron Microscopy (TEM), Energy Dispersive X-ray spectroscopy (EDX) and X-ray Photoelectron Spectroscopy (XPS) measurements. Further investigations into the longevity of the film (target) were conducted using optical microscopy and FTIR spectroscopy. These analyses revealed hydrogenation and oxidation of the film upon exposure to atmosphere, resulting in increased fragility and noticeable colour changes over time.

1. Introduction

Isotopically enriched thin boron targets are required for various nuclear physics experiments using light and heavy ion beams. Boron targets of typical thickness <1 mg/cm^2 are mostly prepared by the vapour deposition and sputtering methods. Vapour deposition by electron beam (e-beam) is commonly used in this regard [1–4]. Similar targets can also be prepared by sputtering with the ion beam [5] and excited plasma [6,7]. For preparation of boron targets with relatively higher thickness (>1 mg/cm^2), techniques like high-energy vibrational powder plating [8,9] and sedimentation [10] are used. Most of the above references have mentioned the difficulties faced during vapour deposition of boron. Difficulties were also faced for other applications requiring boron deposition on different substrates. Techniques used in such applications include thermionic vacuum arc [11], pulsed laser deposition [12] and pulsed magnetron sputtering [13]. The reason behind this difficulty is primarily due to poor thermal conductivity, high melting temperature (2076 °C) and low density (2.3 g/cm^3) of boron. Moreover, boron targets are extremely brittle which creates further hindrance in the preparation of self-supporting targets. Earlier W. D. Riel outlined a few problems and their possible solutions [14]. Due to the high melting point of boron, thin targets are mostly prepared by vapour deposition technique using electron beam. Boron being a sublime material [15] does not pass through liquid phase like other common metallic elements such as Al, Sn, Ag, Au, Bi, etc. This introduces another level of difficulty in the preparation of boron targets. Because of its sublime nature, boron does not evaporate uniformly from the entire sample. Rather it evaporates only from the portion where e-beam hits and creates a crater in the sample. This restricts the fabrication of thick targets and leads to the wastage of costly isotopic enriched materials,

* Corresponding author. Variable Energy Cyclotron Centre, 1/AF Bidhannagar, Kolkata, 700064, India.
E-mail addresses: ruchi@vecc.gov.in (R. Mondal Saha), kaushik@vecc.gov.in (K. Banerjee).

https://doi.org/10.1016/j.vacuum.2024.113642
Received 8 April 2024; Received in revised form 6 September 2024; Accepted 9 September 2024
Available online 14 September 2024

which is highly undesirable.

Wastage also occurs due to the spitting of sublime material, which involves uncontrolled ejection of liquid droplets from the molten evaporant [16]. This effect is more prominent for evaporation done with powder samples. It can produce pin holes or can even destroy the targets. This effect has also been identified previously [1,5]. Traditionally, the spitting effect is minimized by using pellets prepared from the powder sample [17]. In this work we report the development of a new technique where a paste of boron powder was used. Multiple trials were performed to mitigate the problems, as discussed earlier. A comparative study was performed by preparing targets using the paste and the pellet. The relevant causes of the spitting effect were analyzed and possible measures to minimize it are discussed. Requirement of substrate heating during deposition is also discussed for the preparation of self-supported targets. Another important factor i.e. stability of the target is examined and discussed.

2. Description of the apparatus

The apparatus used for fabricating enriched boron targets consists of an electron gun assembly along with four rotational crucible hearths and a substrate holder for placing the glass slides. All these are kept inside a vacuum deposition chamber. A schematic view of the arrangement inside the chamber is shown in Fig. 1(a). A tungsten filament used as a cathode acts as an electron source. A stainless-steel plate situated in front of the filament works as an anode. The potential difference between the two electrodes was 5 kV, which helps to accelerate electrons towards the anode. Finally, the e-beam was deflected by 270° from its initial direction using the magnetic field generated by a permanent magnet. The deflected e-beam hits the boron sample to initiate evaporation by heating beyond its boiling point at vacuum. The substrate holder arrangements for producing carbon(C)/aluminum (Al) backed and self-supported boron targets are shown in Fig. 1(b) and (c), respectively. Details about the two arrangements are discussed in section 3.3.

3. Preparation of enriched boron (^{11,10}B) targets

As discussed in section 1, powder samples cannot be exposed directly to the electron beam for evaporation due to the spitting effect. This would result in a significant loss of material and drop in vacuum level inside the deposition chamber. To overcome these difficulties, boron powder was converted to a paste and pellet. Isotopically enriched boron powders used here were received from the Heavy Water Board, Mumbai. Enrichment of both the powder samples were ~90 % [detail in section 5.2(b)]. Target preparation details along with the challenges faced and their possible solutions are discussed in the following sections.

3.1. Sample preparation

(a) *Paste:* Boron powder was kept in a graphite crucible and anhydrous ethanol was added to it in a drop-wise manner until the whole powder mixed uniformly and produced a paste [see Fig. 2 (a)]. The paste was then tightly pressed inside the crucible with a clean stainless-steel rod with a circular cross section (diameter 10 mm) so that boron powder could be closely packed to avoid spitting during evaporation. Boron paste was left for a few hours so that ethanol evaporated from the paste, otherwise it would lead to degassing during evacuation of the chamber.

(b) *Pellet:* The conventional method of compressing the powder sample at high pressure for producing the pellet was also tried. It

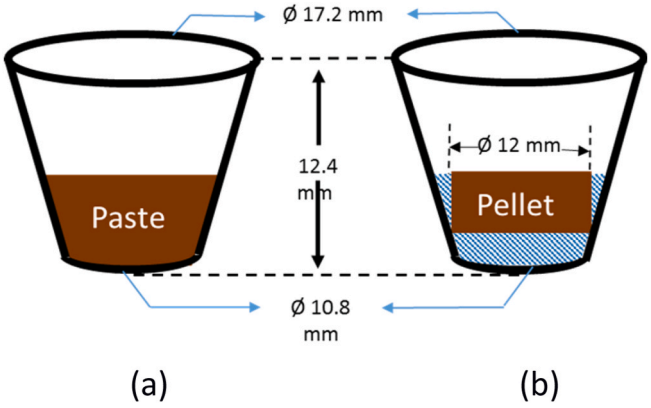

Fig. 2. A schematic diagram of graphite crucible filled with boron (a) paste (b) pellet.

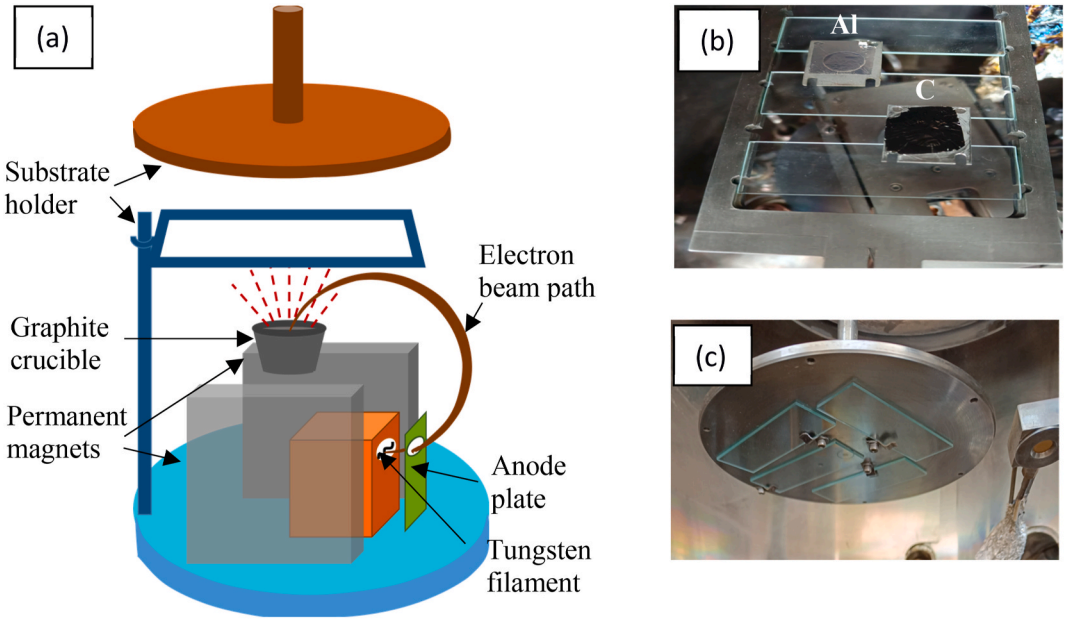

Fig. 1. (a) Schematic view of the components used for the preparation of boron target along with deflected electron beam. Actual photograph of the substrate arrangements used for producing (b) C/Al backed (c) self-supporting targets.

was observed that a pressure of 3 Ton was sufficient to produce boron pellets using a manual hydraulic press. The diameter of the pellet formed was 12 mm.

3.2. Evaporation

A comparative study on the spitting effect was conducted by evaporating boron from both the (a) paste and the (b) pellet forms. To ensure a fair comparison, an equal quantity of material was utilized in both scenarios.

(a) *From paste:*

A boron paste-loaded crucible was placed inside the deposition chamber followed by its evacuation to achieve an air pressure of 10^{-6} mbar. Initially, the paste was heated with an electron beam at low current (1–8 mA). It is important to mention here that evaporation does not take place at this low current. A significant drop in the chamber's vacuum occurred as soon as the sample started heated up. This was possibly due to the degassing and the evaporation of residual ethanol from the boron paste. Once the ethanol evaporated completely and degassing stopped, the vacuum level improved slowly and reached ~5×10^{-6} mbar. The heating of boron paste using the electron beam helped to create a solid lump of boron. Once the lump was formed, current was increased slowly to evaporate material from it. At this high current (50–70 mA) boron started evaporating and the lump eventually transformed into a chunk. The transformation stages of boron powder during electron beam exposure are pictorially shown in Fig. 3.

(b) *From pellet:*

Evaporation from the pellet was also carried out using the same procedure as followed for the paste. During evaporation using pellets there was a risk of sputtering of graphite from the crucible due to the empty space left around the pellet [see shaded region in Fig. 2(b)]. This empty space appeared because of the difference in shapes of crucible (conical) and the pellet (cylindrical). The risk of e-beam hitting on the walls of the graphite crucible further increased due to the steering of the beam on the sample surface during evaporation. However, care was taken to ensure that no damage was caused to the crucible wall. There were cracks observed in the pellet after the evaporation, which is shown in Fig. 3. No such cracks were found in the chunk produced during the evaporation done using the paste.

It is important to note that initial heating and the subsequent evaporation was done in the same chamber without breaking the vacuum for both the cases. This reduced the risk of oxidation of the sample. By comparing both the cases, it was found that the lump and the chunk production time was same for both the samples (see Table 1). The above-mentioned time includes the waiting time to achieve the required vacuum. Procedure adopted to reduce spitting effect during the target preparation from the paste/pellet are summarized as follows:

i. Initial heating of paste/pallet at low current
ii. Step-wise increase of filament current.
iii. Continuous e-beam steering on the sample surface and keeping the exposed area fixed.

3.3. Deposition of boron

Boron deposition from the lump of two different isotopes was done using two different substrate arrangements. ^{11}B deposition was done on thin C/Al foils. Hence, substrate heating was not required. On the other hand, substrate heating was found to be necessary for the deposition of a self-supported ^{10}B target. Hence, two different substrate arrangements were used for ^{11}B and ^{10}B deposition which are described below. Choice of backing/self-supported targets of two different isotopes were random.

(a) ^{11}B deposition on backing foils

Three glass slides were used to hold one C (11 μg/cm^2) and one Al (50 μg/cm^2) foil mounted on a stainless-steel frame [Fig. 1(b)] to be used as backing foils. The gap between the slides were 2 cm from each other. Frame-mounted foils (prepared using the vapour deposition technique) were kept in this gap. The slides were kept at a distance of 10 cm from the crucible loaded with ^{11}B paste. This kind of substrate arrangement can produce targets on different backing elements in a single evaporation.

(b) ^{10}B deposition on the glass substrate

Four glass slides each of area 2.5 cm × 7.5 cm were attached to a circular aluminum holder, which acted as a substrate [see Fig. 1(c)]. The crucible-to-substrate distance was 12 cm. It was fixed to keep the overall solid angle same in both the cases [(a) and (b)]. The distance was increased to compensate for the increase in substrate area. Here, $BaCl_2$

Table 1
Parameter used to produce lump and chunk from boron paste/pellet.

Forms of boron	Beam current (mA)	Exposure time (hrs.)
Lump from paste & pellet	5–7	1.5
Chunk from paste & pellet	8–70	2

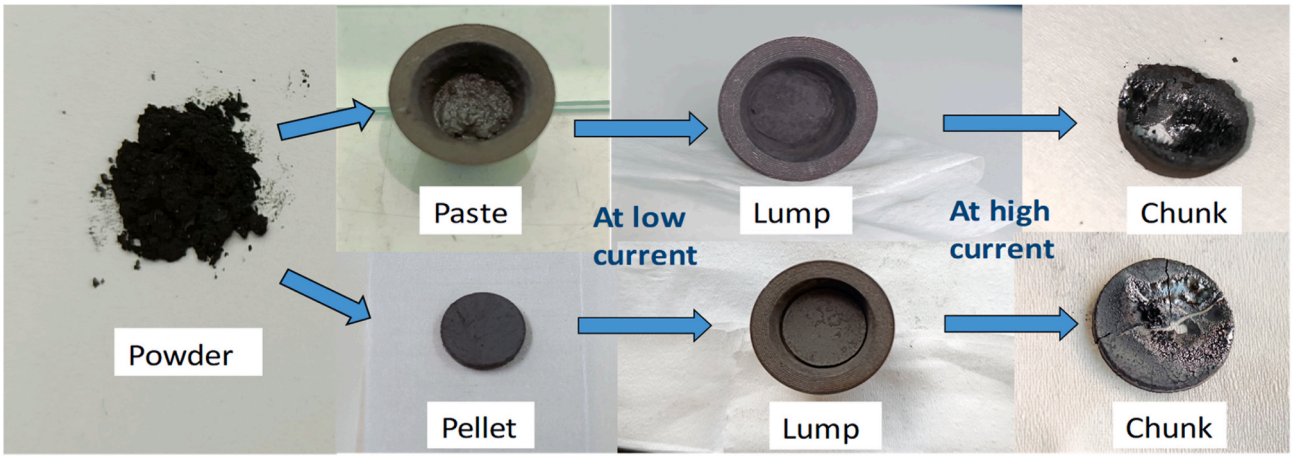

Fig. 3. Different forms of boron samples during target preparation using electron beam.

was used as a releasing agent because of its high melting temperature (962 °C) compared to the other commonly used releasing agents such as teepol (150 °C), NaCl (801 °C) and KI (681 °C). $BaCl_2$ was evaporated initially to produce a layer of typical thickness 20 μg/cm^2 on the glass substrates. After that ^{10}B paste/pellet was exposed to the electron beam to produce a lump. The prepared boron lump was then evaporated by increasing the current up to 70 mA. A lesser thickness was achieved in a longer time duration as compared to the previous evaporation, due to the higher substrate to evaporant distance. Substrates were heated at a temperature of 175 °C during evaporation to reduce the stress on the deposited layer [18]. It is to be noted here, that the use of B_2O_3 as a releasing agent [3,19] can relax the requirement of substrate heating. A layer of B_2O_3 can be prepared by exposing the boron coated glass slides in the ambient atmosphere.

Different parameters used during the deposition are described in Table 2. Deposition time for both cases were found to be higher compared to the time required for the evaporation of usual materials like Al, Sn, Au etc. This is because of its high resistivity towards heat transfer. Another reason was the restricted evaporation rate (0.5–1 Å/s) maintained to avoid the spitting. The quantity of boron consumed for target fabrication was found to be less than 30 % of the material initially taken. This small quantity is because of its poor thermal conductivity. However, the remaining boron sample could be reused for a fresh evaporation. Upon completion of deposition, the chamber was allowed to cool down to room temperature before being vented. Subsequently ^{11}B coated C/Al foils and ^{10}B coated glass slides [Fig. 4(a) and (b)] were taken out from the deposition chamber.

3.4. Effect of substrate heating during film stripping

Stripping of boron layer from the glass slides was required to prepare the self-supported ^{10}B target. Although it is a standard procedure, but certain precautions are required for the boron target preparation, as it is brittle in nature. Any kind of jerking or fast movement of the slides may destroy the thin foils during immersion into the water. So, a custom-designed stand was used to hold the glass slides for better control during the linear and rotational movements. Boron layer was scribed by a surgical knife to get the foils of required area before clamping the slide to the stand. The stand-held glass slide is shown in Fig. 5(a). The slide was placed on a melamine tray filled with distilled water at an angle ~30° with respect to the water surface [20]. The coated slide was then immersed slowly into the water. The level of water then gradually moved upward on the glass slide by melting the $BaCl_2$ layer. This upward rise of water and controlled immersion of the glass slides reduced the stress on the boron layer during its release and floated it smoothly on the water surface. It was observed that the boron layer formed without substrate heating rolled up and tore into small pieces during stripping [see Fig. 5(b)]. This was due to the stress developed on the deposited foil when hot evaporant came in contact with the cold substrate [21]. Once the foil of required area was floated, it was then mounted on an aluminum holder with a hole of diameter 12 mm. Frame-mounted dried ^{10}B foil/target is shown in Fig. 5(c).

4. Thickness measurement

Thickness of the target foils were measured using two different techniques, which are described in the following subsections.

4.1. Crystal oscillation

Thickness of ^{11}B and ^{10}B targets were measured inside the deposition chamber using a digital thickness monitor which consists of a quartz crystal as a basic transducing element. The crystal is excited into mechanical vibration using an external oscillator circuit. Frequency of the oscillation is inversely proportional to the weight of the crystal. Deposition of boron on the surface of the crystal would lower its frequency. The thickness T_k of the evaporated foil was determined by the thickness monitor using the following relation

$$T_k = \frac{N_q \rho}{\rho_f}(t - t_q).$$

where N_q is the frequency of the crystal oscillation, ρ and ρ_f are the density of quartz crystal and the deposited material. The t, t_q are the time period of oscillations for the loaded and unloaded crystal (before deposition) respectively. The measured thickness for both the targets are shown in Table 2.

4.2. Alpha (α)-spectrometry

Thickness of self-supported target (^{10}B) was also determined by measuring energy loss of α particles emitted from a ^{241}Am source [22]. Energy of the α–particles was measured using a silicon surface barrier detector. Thickness measured using this technique was found to be similar with the value measured using crystal oscillation technique (see Table 2). The shift of the α-energy peak due to the target thickness is shown in Fig. 6.

5. Characterization

5.1. Boron powder and electron beam heated sample

To get further insight into the spitting effect boron samples obtained from the different stages of the target preparation were examined using X-ray Diffraction and Fourier Transform Infrared spectroscopy.

(a) X-ray Diffraction (XRD)

X-ray diffraction spectra were measured for the e-beam exposed and unexposed (UE) samples [Fig. 7] in the Bruker D8 Advance X-ray diffractometer using Cu-source. Beam exposed samples can be further classified as direct and indirect exposed (DE and IE) respectively. The central portion of the boron chunk, which was directly exposed to e-beam is termed as direct exposed (DE). Similarly, the peripheral portion of the boron chunk, which was attached to the crucible and indirectly exposed are termed as indirect exposed (IE). XRD of UE samples show two intense peaks at around 15° and 28°, which corresponds to boric acid (H_3BO_3) [23,24] identified using the Crystallographic Open Database (COD) file number 9014010 [25]. It is observed that the H_3BO_3 peaks vanished for the DE samples. Remaining peaks correspond to the β-rhombohedral boron (COD file - 2016171). This indicates a reduction of oxide and hydride of boron in the beam exposed samples. It can be

Table 2
Comparison of different parameters used for the preparation of two isotopic boron targets.

Evaporant	Type of substrate	Substrate to evaporant distance (cm)	e-beam current (mA)	Deposition rate (Å/sec)	Deposition time (hrs.)	Target thickness	
						(μg/cm^2)	(μm)
^{11}B	^{12}C and ^{27}Al	10	16–70	0.1–0.5	1.5	100.0 ± 4.6	0.42 ± 0.02
^{10}B	Glass slides	12	16–70	0.1–0.5	2	75.0 ± 3.0	0.32 ± 0.01

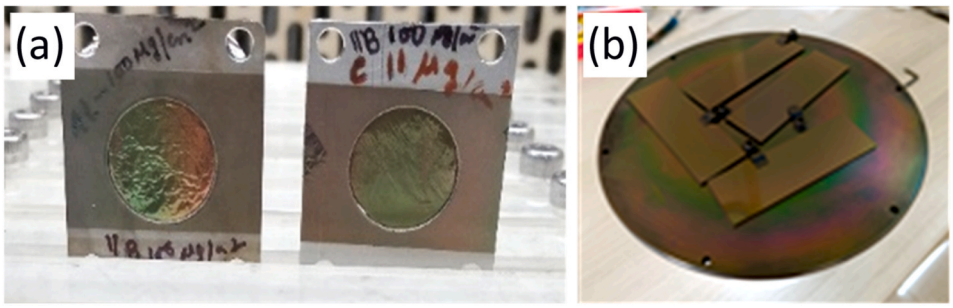

Fig. 4. (a) ^{11}B targets on Al backing (left) and C backing (right). (b) Deposited ^{10}B layer on the glass slides.

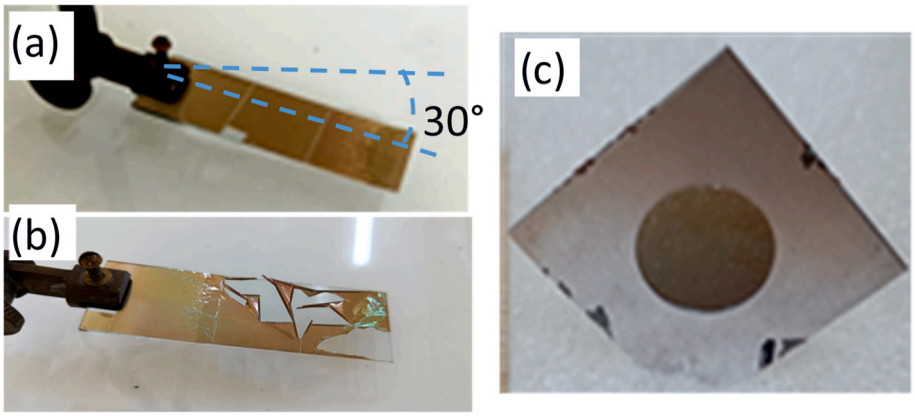

Fig. 5. Stripping of ^{10}B layer prepared (a) with the substrate heating (b) without the substrate heating and (c) frame mounted ^{10}B foil/target.

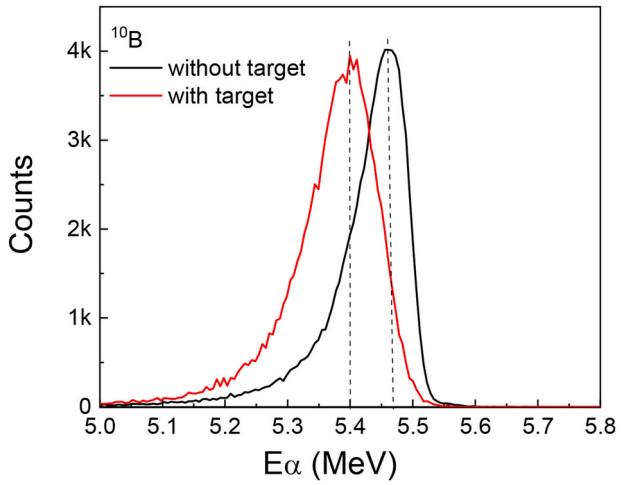

Fig. 6. Measured α-energy spectra for source and the target placed in between the source and the detector.

concluded that e-beam exposure helps to purify and solidify the boron paste/pellet as a chunk and this in turn helps in smoothening the evaporation process by reducing the spitting effect.

(b) Fourier Transform Infrared spectroscopy (FTIR)

Unexposed boron powder and the e-beam exposed samples (chunk) were investigated using the PerkinElmer make FTIR spectrometer Frontier. Sample for this measurement was prepared using the KBr pellet method [26] except for the DE sample. The infrared transmittance spectra for all the samples were taken in the air background, which are shown in Fig. 8. The spectra show a broad band in the wave number

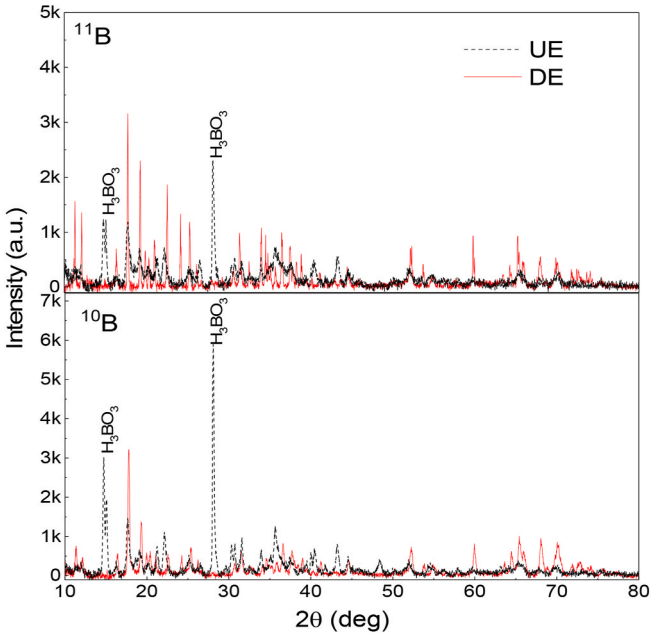

Fig. 7. X-Ray Diffraction spectra of the electron beam exposed (DE) and un-exposed (UE) samples of ^{11,10}B.

(b) Fourier Transform Infrared Spectroscopy (FTIR).

400-860 cm^{-1} for the UE samples of both the isotopes. This can be assigned as O-B-O/B-O-B vibrational bonds [27,28]. Multiple over-lapped peaks from the wave number 860 to 1550 cm^{-1} are mainly due to the B-O bond vibration [29]. The peak at ~1620 cm^{-1} is due to the H_2O bending and the band at ~3500 cm^{-1} corresponds to the O-H/B-OH

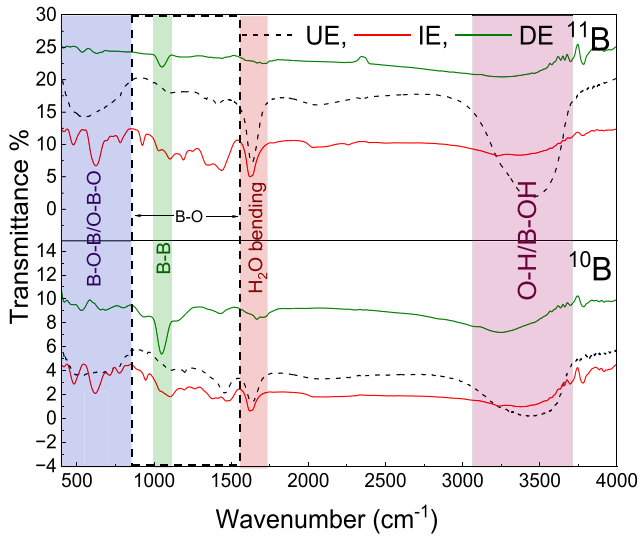

Fig. 8. FTIR spectra of the unexposed (UE), indirect (IE) and directly (DE) electron beam exposed samples of ^{11,10}B. The spectra of DE samples have been scaled down in transmittance for better comparison.

stretching bond [30]. Appearance of O-H and H_2O bonds is partly due to the presence of moisture in KBr salt. The B-O-B, B-O and O-H bonds present in the UE and IE are disappeared in the DE samples. This indicates solidification of boron and removal of the oxygen and hydrogen impurity in the sample on e-beam exposure. The peak at ~1060° cm^{-1} for DE samples was attributed as B-B bond vibration [31]. It has become more prominent in the DE samples, since the other peaks (B-O, B-H) reduced considerably in intensities. This bond appeared due to e-beam exposure at high current.

5.2. Boron deposited layer

After vacuum deposition of boron, the deposited layer was characterized by Transmission Electron Microscopy and X-ray Photoelectron spectroscopy.

(a) *Transmission Electron Microscopy* (TEM)

Boron was first deposited onto a silicon substrate for the TEM measurement, followed by sample preparation using the cross-sectional method [32,33]. This approach was necessary as the original target was extremely thin, which precluded it from undergoing plan-view sample preparation procedures [34]. An FEI TEM (Model No. TecnaiG2 F30S-TWIN) operating at 300 keV was utilized to visualize the magnified structure of the boron layer at the nanometer scale, with imaging facilitated by a Gatan Orius CCD camera.

Bright-field TEM images [Fig. 9(a) and (b)] show a uniform boron layer with a separation on the surface due to oxidation is clearly visible in Fig. 9(b). The spectra obtained from EDX (coupled with the TEM setup) also confirm this fact as oxygen count is higher at the surface compared to inner layer of boron [see Fig. 9(d) and (e)]. SAED patter in the inset of Fig. 9(c) shows amorphous layer. Due to boron's low atomic number (Z), it cannot be detected using EDX. However, analysis of the sample reveals the impurities present in it, which are carbon (C), oxygen (O), silicon (Si), iron (Fe), and nickel (Ni). Oxygen contamination is attributed to exposure to the atmosphere, while carbon may originate from the atmospheric sources or during the sample preparation.

(b) X-ray Photoelectron Spectroscopy (XPS)

Quantitative analysis of the evaporated boron layer was carried out using X-ray photoelectron spectroscopy (XPS) technique. XPS survey spectrum of the evaporated boron layer is shown in Fig. 10(a). In this technique, the bonding of boron with other materials was also explored.

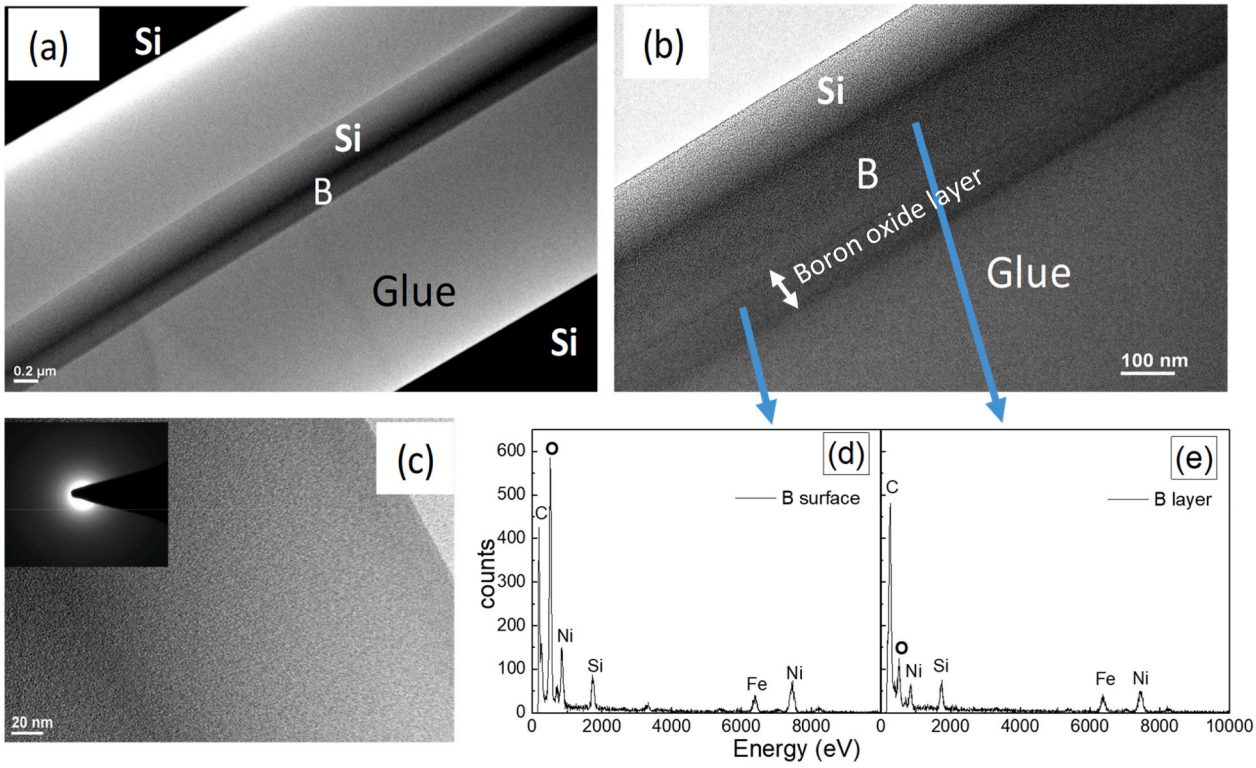

Fig. 9. Cross-section transmission electron microscopy (TEM) bright-field image of the boron surface on Si substrate at (a) 0.2 μ m and (b) 100 nm and (c) 20 nm magnification [inset is the selected area electron diffraction (SAED) pattern from the layer]. EDX spectrum of boron from the (d) surface and (e) interior layer.

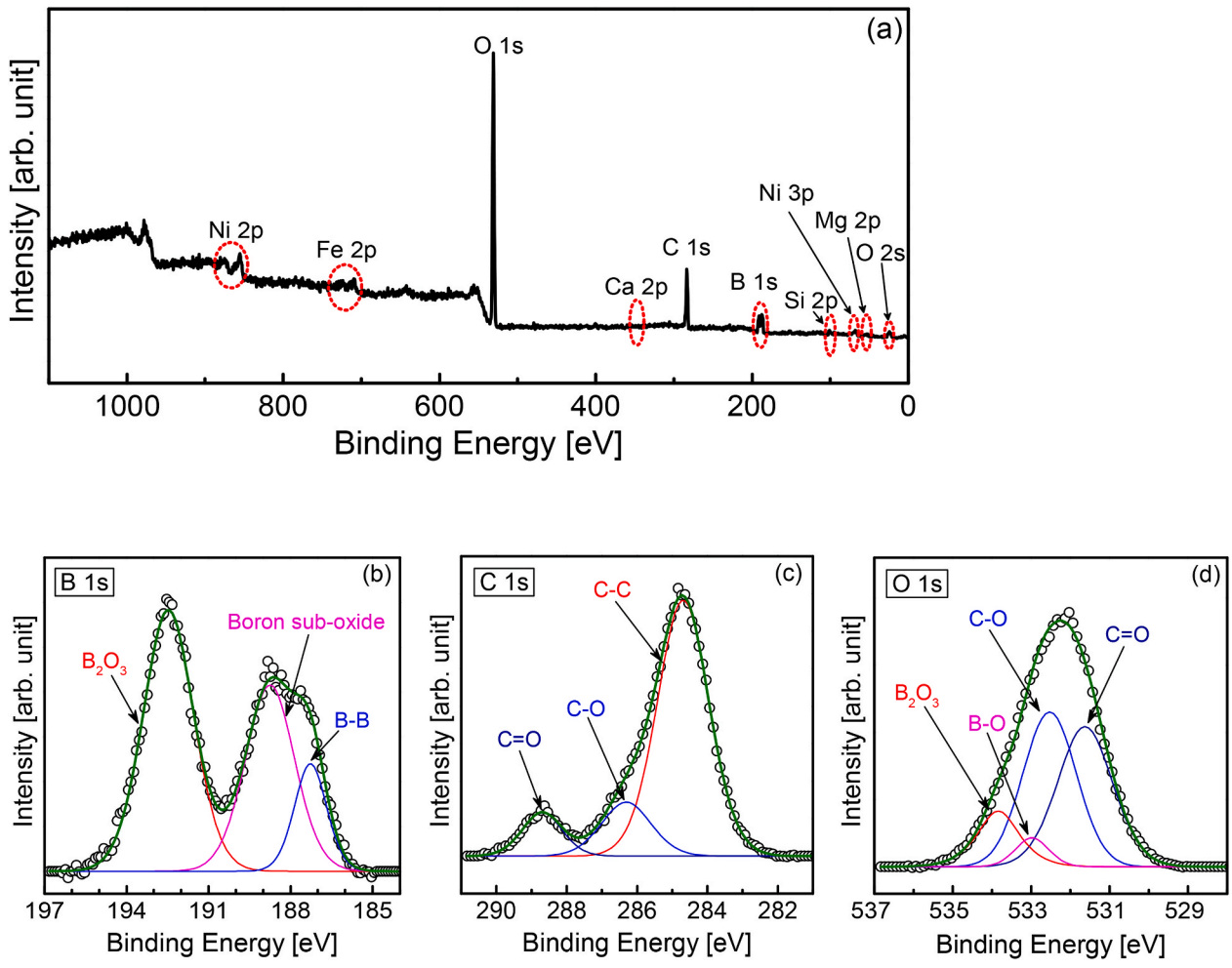

Fig. 10. (a) XPS survey spectrum and (b)–(d) three core level spectra of evaporated boron layer.

For the measurements, first enriched boron powder was evaporated onto a commercially available aluminum foil and then a 1 cm^2 area was cut from that freshly prepared sample and affixed it to a substrate holder. The measurement was conducted in an ultrahigh vacuum chamber (pressure ~ 2×10^{-9} mbar), equipped with an EA125 hemispherical energy analyzer, a monochromatic Al Kα X-ray source (1486.6 eV), a spectrometer with a resolution of ~0.8 eV, and a surface charge neutralizer (Omicron Nanotechnology Ltd., UK) [35,36]. Since boron is a non-conducting material, the surface charge neutralizer was employed during spectrum acquisition. For the analysis, the elemental boron (B-B) peak at 187.3 eV, was used for charge referencing. This peak position (binding energy) was obtained by Ong et al. [37] for surface oxidized β-rhombhohedral boron, without referencing C1s which is generally considered unreliable [38,39]. Since our sample shows similar nature of boron (from TEM and XRD analysis), hence charge referencing based on B-B peak was used. For this, first the B 1s spectrum was fitted freely with three peaks (see Fig. 10(b)) and then the lowest binding energy peak was set at 187.3 eV, corresponding to elemental boron. Accordingly, the higher binding energy peaks at 188.7 eV and 192.5 eV are attributed to boron oxides [37]. Specifically, the peak at 188.7 eV is assigned to boron sub-oxide, where an oxygen atom is coordinated with multiple boron atoms, while the peak at 192.5 eV is assigned to B_2O_3 [37,40]. The core level spectra of C 1s and O 1s are shown in Fig. 10(c) and (d), respectively. The C 1s spectrum is a convolution of three peaks at 284.7, 286.3, and 288.7 eV, arising from C-C, C-O, and C=O, respectively [41,42]. Similarly, the O 1s core level spectrum is a convolution of four peaks, corresponding to C=O at 531.6 eV, C-O at 532.6 eV, B-O at 532.9 eV, and B_2O_3 at 533.8 eV [37,40]. Quantitative analysis of the XPS spectra was also performed to determine the atomic percentage of boron and other impurities in the sample, which are tabulated in Table 3. The calculation excluded oxygen concentration originating from atmospheric sources during the sample preparation. Result indicates that the sample constitutes ~90 % of boron.

Table 3
Atomic percent of the impurities present in the sample.

Name	Atomic %
Si	~ 5
Mg	~ 2
Ni	~ 2
Fe	~ 0.7
Ca	~ 0.5
Total	~ 10.2

6. Target stability

A self-supported ^{10}B and C/Al-backed ^{11}B targets were kept in the ambient atmosphere to check their stability over time. After a period of around one month, ^{10}B target was placed in a vacuum chamber to check its physical stability but unfortunately it could not sustain the stress developed during the chamber evacuation. On the other hand, ^{11}B target turned whitish from its original black colour in a time duration of one year (show in Fig. 11). To investigate these effects both microscopic and

Fig. 11. Actual photographs of ^{11}B target over a period of one year indicates a change in colour.

spectroscopic measurements were performed.

6.1. Optical microscopy

A freshly prepared boron coated glass slide was divided into two parts; one part was kept inside a vacuum chamber ($<10^{-1}$ mbar) and another at the ambient atmosphere. After a month both the parts were investigated using an inverted optical microscope (Carl Zeiss make). Micrographs shown in Fig. 12 indicate a significant difference between the two boron layers. All the images were taken at 20 × magnification. The white regions are more continuous and sharper in Fig. 12(a) (target kept inside vacuum) compared to Fig. 12(b) (target kept outside). These contrasting regions seem to be due to wrinkles present in the film. The film exposed to ambient atmosphere indicates a quicker degradation compared to the film stored under vacuum. Optical micrograph was also taken for a self-supported ^{10}B target kept in the ambient atmosphere for a period of one month. The image shows hills and valleys on the target surface along with tiny pores [Fig. 12(c)]. For qualitative understanding of the above changes, FTIR measurement was performed.

6.2. Fourier Transform Infrared Spectroscopy (FTIR)

FTIR measurement in KBr background was performed to investigate the changes occurred in the boron coated glass slide exposed in ambient atmosphere as a function of time (t). Sample for this measurement was prepared by removing the boron film from the slide and mixed with the KBr salt to form a pellet. FTIR spectra of the air exposed boron films collected for three different time duration are shown in Fig. 13. Peak appearing due to different bond vibrations are marked by the colour bands [31,43–46]. Two intense peaks of O-B-O/B-O-B appeared for the spectrum taken for the sample kept in air for t = 55 days. The intensity of B-B bond appeared in wavenumber 970-1140 cm^{-1} reduced with time. Over the air exposure period, the B-O bond (between 1280 and 1600 cm^{-1}) gradually broadened, and two additional peaks emerged in the spectrum for sample kept in air for 55 days. This new peaks are marked by asterisk in the zoomed portion shown in Fig. 13 (inset). These indicates increased amount of oxygen group in the sample. Broad band

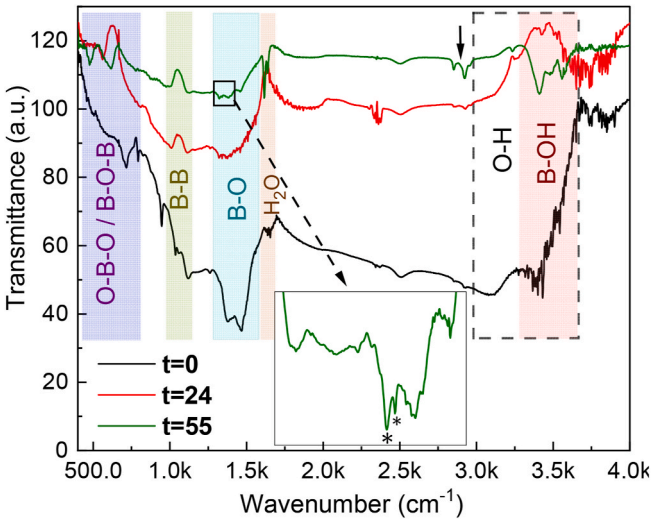

Fig. 13. FTIR spectra of the evaporated boron layer at three different time intervals (in days). Inset figure shows a zoomed-in portion of the spectrum (t = 55 days) marked with square box.

corresponding to the water molecule (O-H) shows a reduction over time, while peaks appearing due to bending vibration of H_2O molecules and B-OH bond becoming intensified, suggesting increasing hydrogen content in the sample. Consequently, peaks marked by solid line arrow also get intense, could be identified as C-H bond and may occur due to the small carbon impurity present in the sample. A quantitative study performed by Nandi et al. showed the formation of H_3BO_3 in amorphous boron by surface oxidation [47]. This study supports our findings regarding the absorption of oxygen and hydrogen by the boron layer upon exposure to the atmosphere. This phenomenon also explains the colour transformation of the target.

7. Conclusion

Carbon/Aluminum backed ^{11}B and self-supported ^{10}B targets were prepared from the isotopically enriched boron powder using vapour deposition technique. The thicknesses of the targets are 100.0 ± 4.6 μg/cm^2 and 75.0 ± 0.3 μg/cm^2 respectively. Use of boron paste and pellet were compared to examine the spitting effect during target preparation. Spitting effect was found to be reduced in both the cases if samples are initially heated at low current. Spitting can be further reduced by increasing the filament current in a step-by-step manner beyond 8 mA. Reason for the reduction in the spitting effect was investigated using X-ray diffraction and Fourier-transform infrared spectroscopy (FTIR). Investigation indicates a significant reduction in the oxide and hydride of boron on electron-beam heating. This in turn helps to solidify the boron sample to produce targets without spitting. The deposited boron

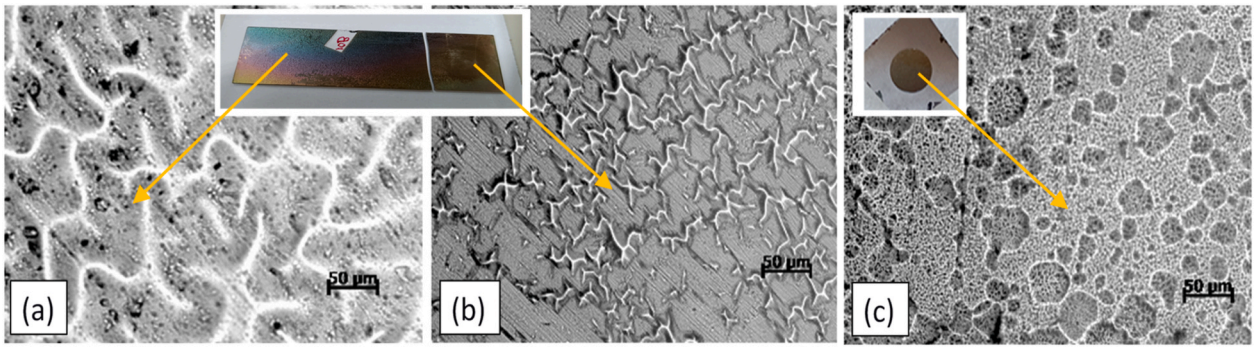

Fig. 12. Optical micrographs of boron layer on the glass slides kept in (a) vacuum (b) ambient atmosphere. (c) Optical micrographs of self-supported target.

layer was examined using Transmission Electron Microscopy and X-ray Photoelectron Spectroscopy analyses. Both reveal a notable concentration of oxygen at the surface layer. The elemental analysis of the sample indicates a ~90 % concentration of boron. Longevity of the target was also investigated using FTIR and optical microscopy which indicates that the target kept in the ambient atmosphere became fragile due to the increased oxygen and hydrogen concentration.

CRediT authorship contribution statement

R. Mondal Saha: Writing – original draft, Methodology, Investigation, Data curation. **K. Banerjee:** Writing – review & editing, Supervision, Methodology, Investigation, Conceptualization. **A. Banerjee:** Writing – review & editing, Resources, Investigation. **N. Gayathri:** Writing – review & editing, Resources, Methodology, Investigation, Formal analysis. **G. Pramanik:** Resources, Investigation, Formal analysis. **Shabi Thankaraj Salammal:** Resources, Formal analysis. **Varsha Agrawal:** Data curation. **Biswarup Satpati:** Resources, Investigation. **Souvik Jana:** Investigation, Data curation. **Satyajit Hazra:** Resources.

Declaration of competing interest

The authors declare that they have no known competing financial interests or personal relationships that could have appeared to influence the work reported in this paper.

Data availability

Data will be made available on request.

References

[1] Laszlo Csihas, Nucl. Instrum. Methods 167 (1979) 171–172.
[2] G.E. Thomas, Nucl. Instrum. Methods A 282 (1989) 124–127.
[3] K. Koide, et al., Nucl. Instrum. Methods Phys. Res. A 370 (1996) 341–344.
[4] J. Greene, et al., EPJ Web Conf. 285 (2023) 10002.
[5] Xu Guo-ji, et al., Nucl. Instrum. Methods Phys. Res. A 397 (1997) 62–63.
[6] Y. Sasamoto, et al., Nucl. Instrum. Methods A 590 (2008) 66–68.
[7] S. Ozawa, et al., Vacuum 74 (2004) 417–421.
[8] A.R. Lipski, et al., Nucl. Instrum. Methods Phys. Res. A 590 (2008) 69–72.
[9] I. Sugai, Nucl. Instrum. Methods Phys. Res. A 397 (1997) 81–90.
[10] R. Mondal Saha, et al., Nucl. Instrum. Methods A 1056 (2023) 168706.
[11] M.Z. Balbag, et al., J. Optoelectron. Adv. Mater. 9 (2007) 858–861.
[12] P. Costa, et al., applied phy A 125 (2019) 99.
[13] M. Audronis, et al., Plasma Process. Polym. 4 (2007) S160–S165.
[14] W.D. Riel, Nucl. Instrum. Methods 167 (1979) 179–181.
[15] E. Vietzke, et al., J. Nucl. Matrls. 196–198 (1992) 1112–1117.
[16] V. Pankov al, Mate. Scie. Tech, 2020, pp. 1743–2847.
[17] P.D. Shidling, et al., Nucl. Instrum. Methods A 590 (2008) 79–82.
[18] G.E. Thomas, Nucl. Instrum. Methods 177 (1980) 591–592.
[19] J.R. Erskine, D.S. Gemmell, Nucl. Instrum. Methods 24 (1963) 397–398.
[20] S.H. Maxman, Nucl. Instrum. Methods 50 (1967) 53–60.
[21] H. Kemi, et al., J. Nucl. Matrls. 266–269 (1999) 1108–1112.
[22] R. Mondal Saha, et al., J. Inst. Met. 16 (2021) T07002.
[23] C. Huber, et al., Energy Sci. Eng. 8 (2020) 1650–1666.
[24] W. Zhang, et al., SpringerPlus 5 (2016) 1202.
[25] http://www.crystallography.net.
[26] L.A. Forato, et al., Anal. Biochem. 259 (1998) 136–141.
[27] J. Li, et al., 016), ISIJ Int. 56 (2016) 752–758.
[28] C. Kayalvizhi, et al., Heliyon 6 (2020) e03133.
[29] C.C. Zhang at al, Catalysts 10 (2020) 1327.
[30] A.L. James, et al., RSC Adv. 7 (2017) 1905–1914.
[31] K. Zielinkiewicz, et al., RSC Adv. 13 (2023) 16907–16914.
[32] Y. Liu, et al., Matrls. Char. 58 (2007) 666–669.
[33] A. Roy, et al., ACS Appl. Mater. Interfaces 9 (2017) 34405–34415.
[34] L.-H. Lee, et al., Ultramicroscopy 197 (2019) 95–99.
[35] S. Jana, et al., Appl. Surf. Sci. 652 (2024) 159368.
[36] S. Mandal, et al., J. Phys. Chem. C 127 (2023) 18176–18184.
[37] C.W. Ong, et al., J. Appl. Phys. 95 (2004) 3527–3534.
[38] G. Greczynski, et al., Nat. Rev. Methods Primers 3 (2023) 40.
[39] G. Greczynski, et al., Prog. Mater. Sci. 107 (2020) 100591.
[40] T.T. Xu Xu, et al., Nano Lett. 4 (2004) 963–968.
[41] B.V. Crist, Handbooks of monochromatic XPS spectra. Volume 2-Commercially Pure Binary Oxides, XPS International LLC, Leona, Tex, USA, 2005.
[42] Z. Wu, et al., Nano Res. 17 (2024) 3053–3060.
[43] A. Aytimur, et al., J. Compos. Mater. 0 (0) (2013) 1–8.
[44] A.S. Kipcak, , et al.Int J. Mate, Metab. Eng. 6 (2012) 7.
[45] J. Zhong, et al., J. Alloys Compd. 607 (2014) 177–182.
[46] Q. Lai, et al., Nanoscale Adv. 1 (2019) 2707–2717.
[47] A.K. Nandi, et al., Cent. Eur. J. Energ. Mater. 9 (4) (2012) 387–398.